

Development of an Ankle Sensor for Ground Reaction Force Measurement in Intelligent Prosthesis

Ali Ihsan Bulbul

Department of Biomedical Engineering, Kocaeli University, Kocaeli, Turkiye
aliihsanbulbul@yahoo.com (corresponding author)

Umut Mayetin

Department of Biomedical Engineering, Kocaeli University, Kocaeli, Turkiye
umayetin41@gmail.com

Serdar Kucuk

Department of Biomedical Engineering, Kocaeli University, Kocaeli, Turkiye
skucuk@kocaeli.edu.tr

Received: 7 April 2024 | Revised: 23 April 2024 | Accepted: 24 April 2024

Licensed under a CC-BY 4.0 license | Copyright (c) by the authors | DOI: <https://doi.org/10.48084/etasr.7430>

ABSTRACT

In this study, a new low-cost, three-degree-of-freedom force sensor is developed to measure Ground Reaction Forces (GRFs) and to be used in the safe control of active transfemoral prosthesis. Initially, the proposed sensor was designed with the Finite Element Method (FEM). Then, the sensor's control board was developed to include an electronic circuit with its microcontroller module, four load cell amplifiers, and an orientation sensor. A test platform was also developed to conduct the sensor tests. To test the accuracy of the results obtained from the developed test platform, the same tests were also carried out with a commercial sensor and similar results were obtained, thus proving that the sensor is suitable for use in prosthetics.

Keywords-active transfemoral prosthesis; control; control board; Finite Element Method (FEM); force sensor; ground reaction forces; test platform

I. INTRODUCTION

Amputation is the severance of a limb, at any level, from the body. [1]. About 1.9 million people in the world have lost their legs for various reasons, and it has been found that about 400 thousand of these people have above-the-knee amputations [2]. Lower limb (transfemoral) amputation has a serious impact on a person's physical activity. The loss of a leg is a traumatic condition and causes a loss of freedom, as it reduces functional capacity and excludes an individual from life [3-8]. Amputee rehabilitation aims to improve function and life quality. Transfemoral prostheses act as a treatment for amputations or congenital missing legs [9, 10]. Transfemoral prostheses can be of two types: active and passive. Passive prostheses do not provide any moving support, whereas the active ones offer active support for their user to move in the desired trajectory [11-14].

Since the transfemoral prosthetic contacts touch the ground, their employment requires force control. Especially in active prostheses, it is important to control the prosthesis with an effective control method. For safe movement, the forces

applied to the prosthesis are measured and exploited to regulate the prosthesis [15, 16] like in other biorobotic applications [17-19]. The natural balancing system of the human body is controlled by the muscles and bones. Prosthetic members disrupt the natural functioning of this balancing system, and prosthetic users cannot percept accurate feedback about the reaction forces. In this case, user safety may be compromised. Sensors have an important statue in solving this issue. They can be deployed for safe control of active transfemoral prosthesis, while they have a primary role in improving correct gait and prosthetic fit [20-22]. A sensor is a key element in the prosthesis structure, used in the control of the prosthesis.

The reactions of the active prosthesis in contact should be compatible with the normal leg and the user's intention. Therefore, Ground Reaction Forces (GRFs) are put into service for the measurement of contact forces. The correct adjustment of the prosthesis is very important in providing comfort and harmony during its utilization. A significant part of the transfemoral prosthetic sensors is that they are used to compute the ground reaction forces during the body movements of the

prosthesis user. These sensors can be deployed to record the gait data of the prosthetic user and help with the correct control and adjustment of the prosthesis. They can also provide data to the developed controllers. Therefore, the measurement of the GRF is substantial in controlling both the above-knee and below-knee lower limb prostheses [23, 24]. There are professional and expensive sensors that can be applied for the calculation of GRFs [25]. However, is impractical to use expensive general-purpose sensors in lower limb prostheses, since they do not physically adapt to the prostheses. Additionally, high-cost commercial sensors increase the cost of prosthetics. This is a significant obstacle to the widespread prosthesis usage. The sensor is usually positioned between the ankle and foot for force control.

The study described in this article presents the sensor feasibility required for the design of a transfemoral prosthesis. The developed transfemoral prosthesis and sensor design are shown in Figure 1. With the active knee and ankle prosthesis considered, the aim is to provide improved functional support compared to passive prostheses. The designed transfemoral prosthesis, observed in Figure 1, has the potential for balance advantage on rough ground with three-axis movement by the designed sensor.

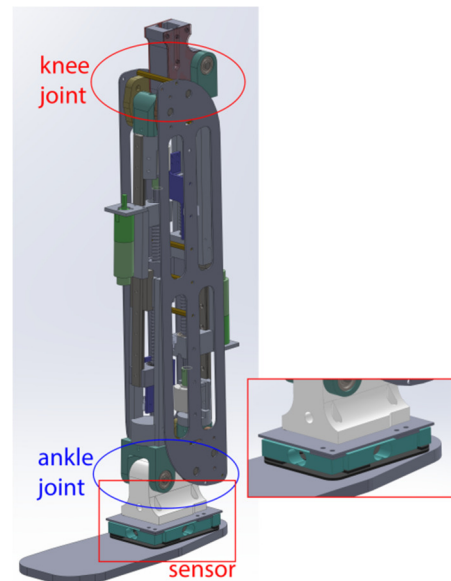


Fig. 1. Transfemoral active prosthesis design and the proposed sensor.

TABLE I. COMPARISON OF COMMERCIAL AND NON-COMMERCIAL FORCE SENSORS

Reference	Measurement capability	Design purpose	Measurement approach	Measured values	Dimensions (mm)	Cost	Electronics
[36]	3 axis force, 3 axis torque	General robotics	Piezoresistive	General	q25 × 21.6	Very high	Separated
[35]	3 axis force	Gait analysis	Piezoresistive	GRF, CoP	Dispersed	Lower	Separated
[37]	3 axis force, 3 axis torque	Daily activity and gait analysis	Piezoresistive	GRF, CoP	q45 × 15.7	Very high	Separated
[31]	3 axis force, 3 axis torque	Gait analysis	Piezoresistive	ZMP, GRF	2 pieces	Higher	Separated
[32]	3 axis force	Gait analysis	Piezoresistive	GRF, CoP	280 × 120 × 43	Higher	Integrated
[34]	3 axis force, 3 axis torque	General robotics	Piezoresistive	GRF	Dispersed	Lower	Separated
[38]	3 axis force	Gait analysis	Optical	GRF	Dispersed	Higher	Separated
[23]	3 axis force, 3 axis torque	Below knee prosthesis	Piezoresistive	GRF, ZMP	45 × 45 × 9	Very high	Integrated
[39]	3 axis force, 3 axis torque	Transfemoral prosthesis	Piezoresistive	GRF	q94.5 × 33,3	Higher	Separated
[40]	2 axis force	Transfemoral prosthesis	Piezoresistive	GRF	q100 × 40	Higher	Integrated
[41]	2 axis force	Movement analysis	Optical	GRF	50 × 50 × 35	Higher	Separated
Proposed	3 axis force	Transfemoral prosthesis	Piezoresistive	GRF, CoP, ZMP	130 × 80 × 24.7	Lower	Integrated

The force between the prosthesis and the ground is detected by a sensor. Thus, the movement of the active transfemoral prosthesis is managed by the sensor [15, 16, 20, 26]. According to biomechanical data, there is an average GRF of 1000 N for a healthy person [27-29]. In order for the sensor to be used in a transfemoral prosthesis, it must meet these requirements. The sensor in [30] is positioned under the foot for a lower limb-like anthropomorphic robot. The former is designed as a three-axis moment to recreate the Center of Pressure (CoP). The sensor under the universal joint, which is the ankle joint, has been employed as a determinant in the robot's walking by measuring force and moment on three axes. In [31], a six-axis force sensor was developed for estimating GRFs in humans or humanoid robots. The sensors were connected with parallel support. In [32], a low-cost sensor package was introduced for clinical gait analysis that can provide quantitative and reproducible results. Force sensing resistors and piezoelectric sensors were implemented for force measurement. In [33], a force sensor with 6 degrees of freedom was developed. Sixteen Strain Gauges (SGs) were utilized in the sensor to detect the Center of

Pressure (CoP) and Zero Moment Point (ZMP) for gait analysis. A sensor package with nine SGs designed for gait analysis was also flexibly mounted under the shoe [34]. Authors in [35] proposed a wearable sensor designed to measure the GRF. Gait analysis was adopted to measure the pressure center [35]. The sensor system includes five small three-axis force sensors that come under the foot. Single-axis transfemoral prosthesis studies predominate in the literature and commercial products. The freedom of movement of these prostheses is limited. Especially in commercial prostheses, sensors are generally not used.

Table I portrays a comparison of commercial and non-commercial force sensors. The comparison is performed taking the following issues of the sensors into consideration: Measurement capability, design purpose, measurement approach, measured values, dimensions, producing cost, and electronics.

In particular, the following sensors were evaluated. They have been developed for the computation of the described

GRF, CoP, and ZMP values. Similar studies are excluded and the most characteristic ones are expressed. Most of the sensors in Table I are developed for general purpose applications and only four are developed specifically for prosthetic purposes. The majority of sensors perform measurements based on the piezoresistive effect, and a few sensors also carry out optical measurements. The force sensors in Table I have different sizes. The proposed sensor in this study is designed in dimensions suitable for use in prosthetics.

Considering Table I, the sensor package in this study differs from the sensors developed for force measurement in the literature. The former sensor is designed in accordance with the transfemoral prosthesis structure in Figure 1 and the GRF measurement requirement. Almost all prostheses are different from each other. Therefore, the sensor design is unique to itself, as in the prosthesis. The proposed sensor is a cost-effective modular design developed as an alternative to expensive multi-axis force sensors, and thus more amputees can be reached with the modular structure and low cost features of the designed sensor. The sensor's sensing capabilities can be extended according to the user needs by easily switching individual load cells. This renders the recommended sensor a modular structured sensor the modular design of which makes it simpler to be manufactured and installed. As expressed in Table I, the sensor-specific control card is integrated with the mechanical design. As noticed in Figure 1, the sensor under the ankle joint is physically small and lightweight. The proposed sensor (i) is specifically designed for prosthetics and GRF measurement, (ii) has low cost, (iii) has less producing and assembly complexity, (iv) has a modular structure, and (v) has an integrated structure.

The sensor package designed in this study includes lower and upper layers, load cells combined in a modular structure, and a control card. The sensor package is a 3-axis force sensor for GRF measurement, which is especially needed in transfemoral prostheses. The structural design of the suggested sensor was executed following the Finite Element Method (FEM). A test platform suitable for the intended use for sensor tests has also been developed. The measurement protocol appropriate for the needs of the prosthetics was applied to the sensor on the test platform. Basic sensor tests were performed and the results were verified by comparison with those of a commercial sensor.

II. PRINCIPLES OF MEASUREMENT

Many methods have been implemented to measure the forces exerted to objects. The use of load cells is the most common one. A load cell converts a load force into an electrical signal using piezoresistive SGs. The latter are employed to obtain expansion or contraction data of the materials subjected to any force. A load cell unit has four SGs placed to the upper and bottom surfaces, as depicted in Figure 2. The load cell is fixed at a certain side and the force is applied at the opposite side. When a force is applied (Figure 2), SG1 and SG3 are under tension, whereas SG2 and SG4 are under compression. Tension or compression effects (either positive or negative), change the shape of the SG and this alteration is expressed as strain. Thus, the tension and compression effects lead to a strain in each of the four SGs. Using the strains that a

load cell will generate under a certain force, the total strain ε of the load cell can be calculated by [39, 40]:

$$\varepsilon = \varepsilon_{sg1} - \varepsilon_{sg2} + \varepsilon_{sg3} - \varepsilon_{sg4} \quad (1)$$

where ε is the total strain of the load cell and ε_{sg1} , ε_{sg2} , ε_{sg3} , and ε_{sg4} are the strains formed in the SGs in the load cell. The SGs are attached in the form of a Wheatstone bridge as displayed in Figure 2. Therefore, an electrical signal proportional to the applied load is obtained from the SGs.

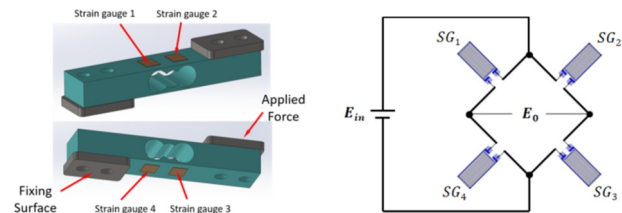


Fig. 2. The single load cell unit, placement of the four SGs, connection of the SGs.

The load cell is mounted on the element where the force is detected and is exposed to the change caused by its deformation. The main variable about the strain sensitivity of load cells is the Gauge Factor (K).

$$K = \frac{\Delta R / R}{\Delta l / l} = \frac{\Delta R / R}{\varepsilon} \quad (2)$$

where R is the resistance, l is the length and ε is the strain. In general, the strain on the force sensing element is very small. The change in resistance is less than 0.2% [41].

The output can be calculated deploying the Gauge Factor and by the following equation as the ratio between the voltages:

$$\frac{E_o}{E_i} = \frac{1}{4} K \varepsilon \quad (3)$$

where E_i and E_o represent the input and output voltage of the Wheatstone bridge, K is the Gauge Factor (about 2.0), and ε is the total strain of the single load cell unit. From (3), the output voltage has a linear relationship with strain.

III. STRUCTURAL DESIGN

The sensor has four load cells positioned between the ankle and the foot for force control. The sensor package includes two lower and upper laser-cut 7075 Al sheet plates. They are connected for load distribution and to operate as unifiers. Four load cells are positioned between these plates. The load cells (Uxcell, a18112500ux0206) are combined in the structure presented in Figure 3 to measure the ground reaction forces in the sagittal and frontal planes. There are spacers manufactured with a 3D printer from carbon fiber ABS material that help to make connections between the plates and the load cells. The sheet metal sheets have dimensions of 80 mm \times 130 mm and the total height of the sensor with sheet metal sheets, carbon fiber ABS parts and load cells is 24.70 mm. The parts are connected to each other with screws.

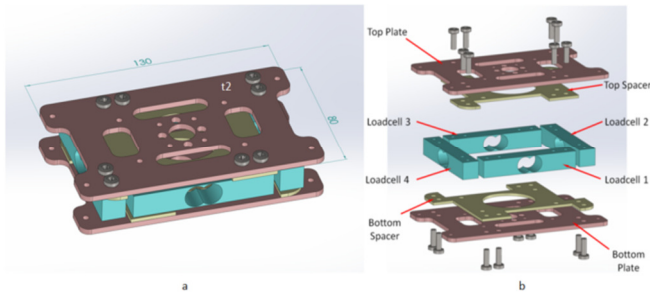


Fig. 3. Sensor package design and dimensions, (a) assembly view, (b) exploded view.

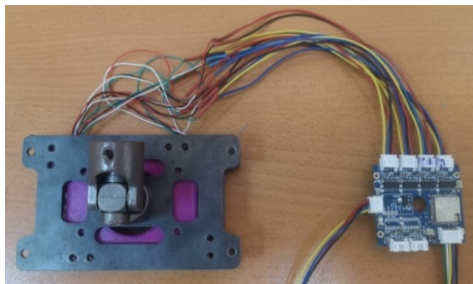


Fig. 4. Sensor package and control card.

An electronic board containing the ESP32-WROOM-32UE microcontroller module and an ADS1256 24 bit 8 channel analog to digital converter is developed to acquire the sensor data as depicted in Figure 4. This board also includes a smart 9-axis orientation sensor of BNO055, which has a three-axis 14-bit accelerometer, a three-axis 16-bit gyroscope, a three-axis geomagnetic sensor, and a 32-bit microcontroller. The block diagram of the control board for the proposed sensor package is observed in Figure 5. This board has small dimensions and low energy consumption. Small size is an important advantage because it allows easy placement into the body of the prosthetic user.

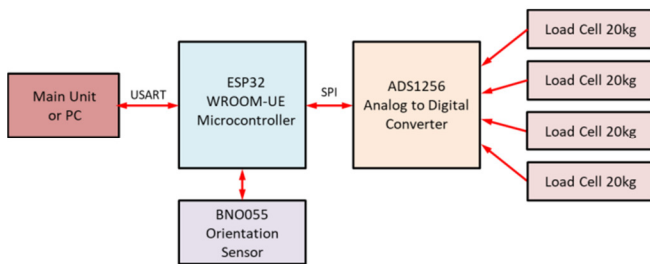


Fig. 5. Sensor package and control card.

TABLE II. PROPOSED SENSOR PRODUCTION COST

Part	Manufacturing	Pieces	Dimensions	Price (\$)
7075 Al Sheets	Laser cutting	2	80 × 160 × 2 mm	6
Load cells	Bought	4	45 × 6 × 9.40 mm	8
ESP32-WROOM	Bought	1	-	4
ADS1256	Bought	1	-	15
PCB	Sample design	1	40 × 36 mm	4
Other electronic components	Bought	-	-	2
Total cost				39

Multi-axis force sensors available in the industry cost between one thousand and ten thousand dollars. Table II manifests the cost items of the proposed force sensor in detail. The total cost of the multi-axis force sensor proposed in this study is around \$40, including the produced mechanical and electronic parts.

IV. MECHANICAL (STRAIN) ANALYSIS

This section presents the finite element analysis of the sensor. The ANSYS software was implemented for the FEM modeling. Figure 6 illustrates the 3D shape and finite element model of the sensor components. The sensor consists of 713575 elements and 1647977 nodes. The element size in the model is 0.5 mm. The forces are exerted to the upper plates by fixing the sensor lower plates as evidenced in Figure 7. The mechanical properties of the lower and upper plates are determined as that of the 7075 Al sheet material. Carbon fiber ABS mechanical properties are identified for the 3D printed and connected to the metal sheet parts. The mechanical properties of the 7075T7441 aluminum alloy are determined from the load cell datasheet.

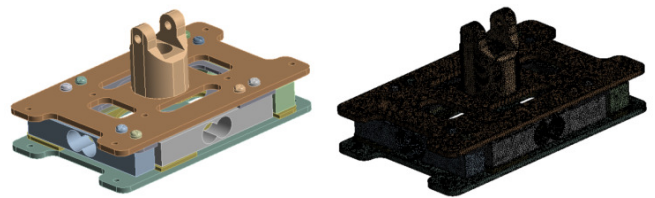


Fig. 6. 3D and finite element model of sensor components.

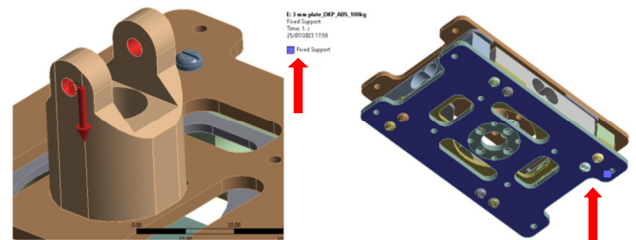


Fig. 7. Exerting force to the sensor, force direction, and fixed support.

TABLE III. FINITE ELEMENT ANALYSIS

Material type	Measurement results (MPa)	Critical value (Maximum strength) (MPa)
Load cells	351.37	525
Carbon fiber ABS	25.61	54
Sheet plates	215.45	420

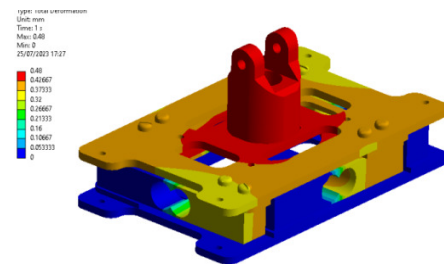


Fig. 8. Total deformation.

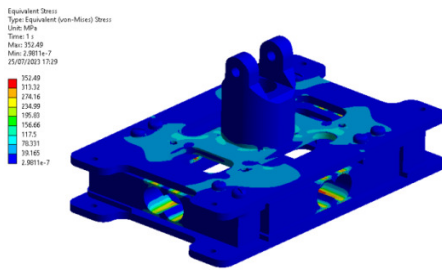


Fig. 9. Von Mises strain distribution.

The design of the sensor structure is essential for a force sensor, because the accuracy and sensitivity of the sensor are greatly related with the structure. Figures 8 and 9 demonstrate the strain distributions on the designed sensor from FEM analysis. The total deformation is 0.48 mm. The security coefficient is 1.49. According to the FEM results, the design is highly durable. The results of von Mises stress in Table III were acquired by the FEM analysis. The former exhibit a satisfactory accuracy of the proposed sensor according to the defined boundary conditions.

V. TEST PLATFORM

A test platform was constructed to estimate the performance of the sensor package as revealed in Figure 10. A universal joint was located on the top plate of the sensor package to hang up lower leg weights. Thus, this platform provides the angles required for the prosthesis. The movements that occur at the ankle joint are plantar flexion, dorsiflexion, inversion, and eversion. The motion ranges are: dorsiflexion 30°, plantarflexion 50°, inversion 35°, and eversion 20° [45]. The platform supports these angles to prove measurements in the sagittal and frontal planes.

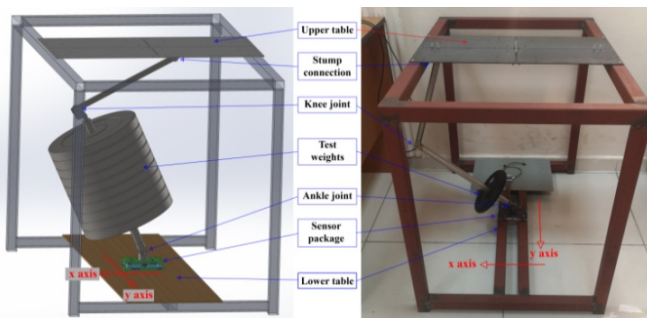


Fig. 10. Test mechanism.

The angles made by human knee and ankle joints can be simulated with the two-joint structure. The two-joint structure is mounted by hanging on the upper table in the test mechanism. The lower and upper axes are connected to each other by vertical fittings. Thus, axis shift is prevented at the lower and upper connection points. There are connection holes made by laser cutting at equal distances on the x and y axes on the upper table. The connection point to the upper table can be connected through the desired hole depending on the need. Thus, dorsiflexion-plantarflexion movements on the x axis and inversion-eversion movements on the y axis can be applied at the desired angle. The sensor package is fixed to the lower

table to prevent the drift effect. Accurate force measurements can be made with the fixed sensor. The load to be mounted on the sensor is controlled by using fixed weights. Since the sensor package is intended to be utilized in transfemoral prosthesis, a maximum user weight of 80 kg has been determined. For example, during walking, the weight will ride on the prosthesis. The sensor package can compute the forces caused by different weights. For this purpose, the knee joint can be easily separated by means of a pin, whereas it is possible to be reconnected through loading different weights.

In the test mechanism, the knee joint and the hanger system are capable of moving on one axis (1 DOF), whereas the ankle joint is designed to have freedom of movement on two axes (2 DOF) with a universal joint. Thus, by controlling the joints, the movement at the ankle joint can be simulated.

VI. FORCE SENSING

Zero balance of force sensing is needed to initiate the calibration measurement. The force sensing unit consists of piezo-resistive load cells and the zero point of drift caused by some environment variables can be spotted in the measurement values. These drift values are in very low range, because the sensor unit is used with limited temperature degrees and they are eliminated through a calibration algorithm. Thus, the measured value equals to 0 when no load is applied to the force transducer. It is ensured that all parts are tightly assembled into one unit. Then, the force is increased to the nominal value, while the output signal is observed. The difference of the output signal between zero force and the nominal force gives the rated value.

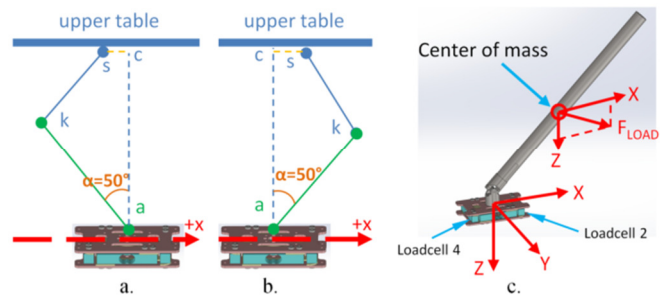


Fig. 11. Force tests for ankle joint on the x-axis (a) $\alpha = -50^\circ$, (b) $\alpha = 50^\circ$, (c) load cell placement on the x-axis.

Static forces are exerted to determine the linearity and sensitivity of the sensor. Each force is exerted to the sensor at different angles, from zero to full-scale value. Maximum angles for dorsi-plantar flexion and eversion-inversion movements at the ankle are 50° and 35°, respectively. The force sensor tests are performed with these angles. The α angles on the x-axis can be detected in Figure 11. The connection points providing these angles are calculated by using the shift values from the upper table center.

The terms of s, k, and a represent the stump connection point, knee joint, and ankle joint, respectively (Figure 11). When a force is exerted to the sensor on the x-axis, the difference between the measurements of the load cells loadcell 2 and loadcell 4 gives the F_x value. Similarly, when a force is

exerted to the sensor on y-axis (Figure 12), the difference among the measurements of the load cells, loadcell1, and loadcell3 gives the F_y value. The β angles on the y-axis can be evidenced in Figure 12.

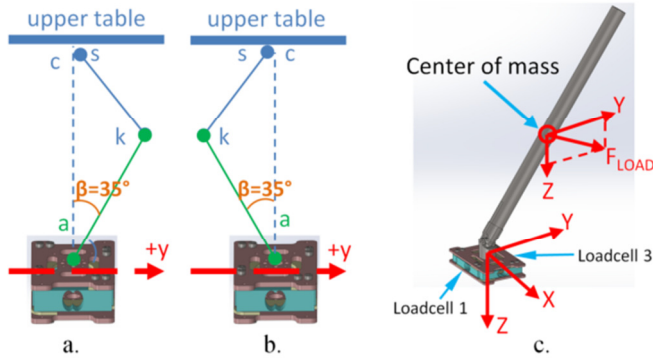


Fig. 12. Force tests for ankle joint on the y-axis: (a) $\beta=35^\circ$, (b) $\beta=-35^\circ$, (c) load cell placements on the y-axis.

Firstly, the forces are exerted to the sensor in the vertical direction (z axis) using bumper plates. The weights of the plates are 0, 5, 10, 15, and 20 kg for the loading process and the same in reverse for the unloading process. The bumper plates are weighed with a precision scale. This is the test protocol repeated in the test platform by exerting force to the sensor at the above given angles. Hysteresis, repeatability, and linearity tests are also performed on the sensor with this method.

Table IV exhibits the nominal output of the FEM and the experimental results according to the weight of 20 Kg (190.43 N) with angles of 50° on the x axis and 35° on the y axis (Figures 11, 12). The FEM output values are computed with (3) from the strain data obtained with FEM. The errors of the characteristic test results acquired from the FEM analysis are 0.7% for F_x and 2.6% for F_y . Errors are caused by position errors of the load cells, production error of lower and upper layers, and the FEM software.

TABLE IV. NOMINAL OUTPUT OF SENSOR PACKAGE FROM FEM AND CHARACTERISTIC TEST RESULTS

Force (190.43 N)	Output rate (mV/V)		Error (%)
	FEM	Experimental	
F_x	-0.45	-0.453	0.7
F_y	0.87	0.847	2.6

A weight of 20 Kg (190.43N) is employed to measure the interference error of sensor package, and its results are given in Table V. As described above, the interference error is evaluated by the forces exerted on the x and y axes at the determined angles. As demonstrated in Table V and as expected, the error is higher on the y axis than on the x axis, because the load cell positions in the sensor structure (Figures 3, 11, and 12) are different on the x and y axes. Therefore, the maximum interference error of the developed sensor is 1.86%.

Forces in the loading and unloading processes are exerted to the sensor applying the described protocol. The sensor output voltages on the x and y axes are measured for all forces and the results are graphically provided in Figure 13.

TABLE V. INTERFERENCE ERROR OF SENSOR PACKAGE FROM FEM

Force (190.43 N)	Interference error (%)	
	F_x	F_y
F_x	-	0.21
F_y	1.86	-

The F_x values increase as the force increases on the x axis. Similarly, they decrease as the force decreases on the x axis. The measurement results have linear characteristics proportional to the input force. Meanwhile, as the force rose and was reduced on the x axis, the F_y values were measured close to 0, as expected. Deploying the same protocol, the sensor was tested at a 35° angle on the y axis and the negative y-axis. The sensor output voltages on the x and y axes are computed for all forces and the results are graphically showcased in Figure 14.

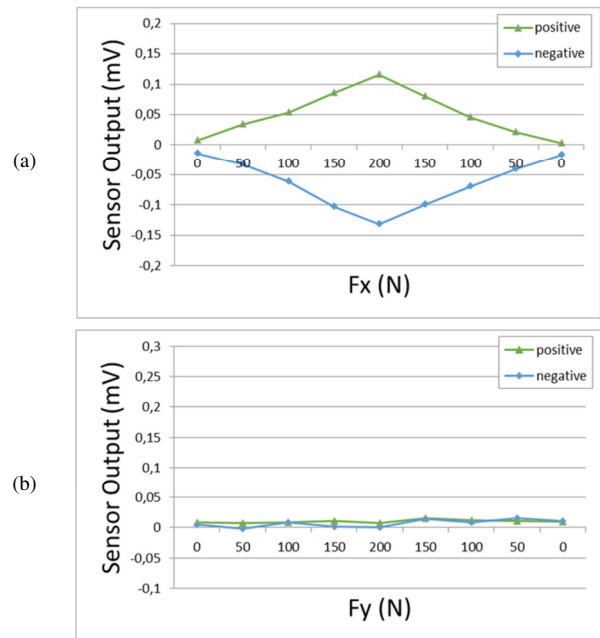


Fig. 13. Results on the positive (in green) and negative (in blue) x-axis, when loading and unloading. (a) F_x values, (b) F_y values.

The F_y values increase as the force increases on the y axis and decrease as it decreases. However, as the force increased and decreased on the y axis, the F_x values were measured close to 0, as anticipated. The measurements seen in Figures 13 and 14 are attained by exerting forces to the sensor at certain angles. The graphs show the linearity in the measurements. Additionally, hysteresis error is measured during the loading process for the sensor package. The forces are exerted to the sensor package vertically on the z axis with increasing values. The results and errors are disclosed in Table VI. The highest error value is 0.75% and the lowest is 0.10%. The hysteresis error is in the range of 0.65%. In addition, in the measurements, the decreasing error rate values are obtained with an increasing load. Regarding these results, it can be concluded that the sensor has a high hysteresis-free performance.

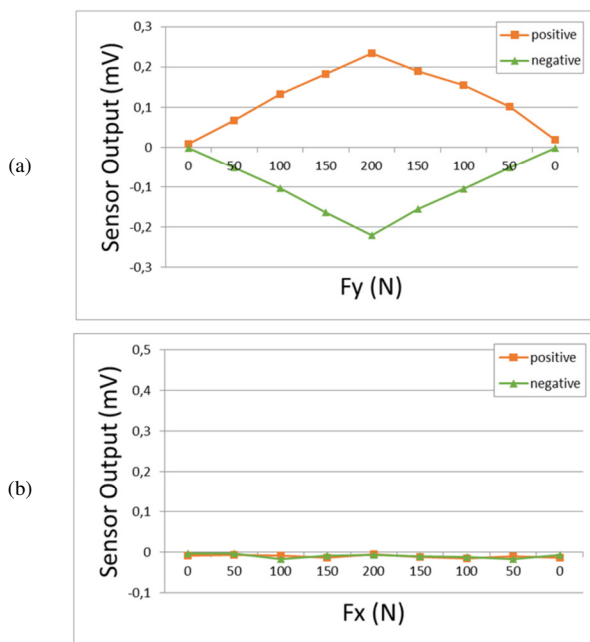


Fig. 14. Results on the positive (in orange) and negative (in green) y-axis when loading and unloading. (a) Fy values (b) Fx values.

TABLE VI. HYSTERESIS ERROR OF SENSOR PACKAGE

Fz (N) Reference	Fz (N) Experimental	Error (%)
47.02 N (5 kg)	46.67	0.75
93.91 N (10 kg)	93.26	0.69
143.06 N (15 kg)	142.92	0.10
190.43 N (20 kg)	189.59	0.44

The designed sensor was also subjected to repeatability testing. Figure 15 depicts the outcomes of exerting 190.43N (20 kg) force 20 times on the three-axes. The force was applied vertically in the z-axis and at certain angles on the x and y axes as described above. Sensor repeatability error is the highest at 1.063% on the x-axis, 0.639% on the y-axis, and 0.466% on the z-axis.

In general, errors are caused by certain reasons. One of them is the thickness of the processing plate, considering the production of the lower and upper tables of the sensor. The rigidity of the sensor's assembly and the manufacturing precision of the parts ensure high accuracy results. Mass production errors of the load cells effect interference errors. Other reasons can be the errors generated by the mounting of the sensor parts, errors from control board, and errors from temperature variation. Concerning the comparative FEM analysis and the experimental results, the sensor can be characterized as suitable for transfemoral prosthesis.

VII. VERIFICATION

An ATI F/T Gamma SI-65-5 sensor was used for the verification of the proposed sensor package. The latter was compared with the ATI sensor taking into account static measurements. The ATI sensor has measurement limits of 65 Nm for x and y axes, 200 Nm for the z axis, and 5 Nm torque for all axes.

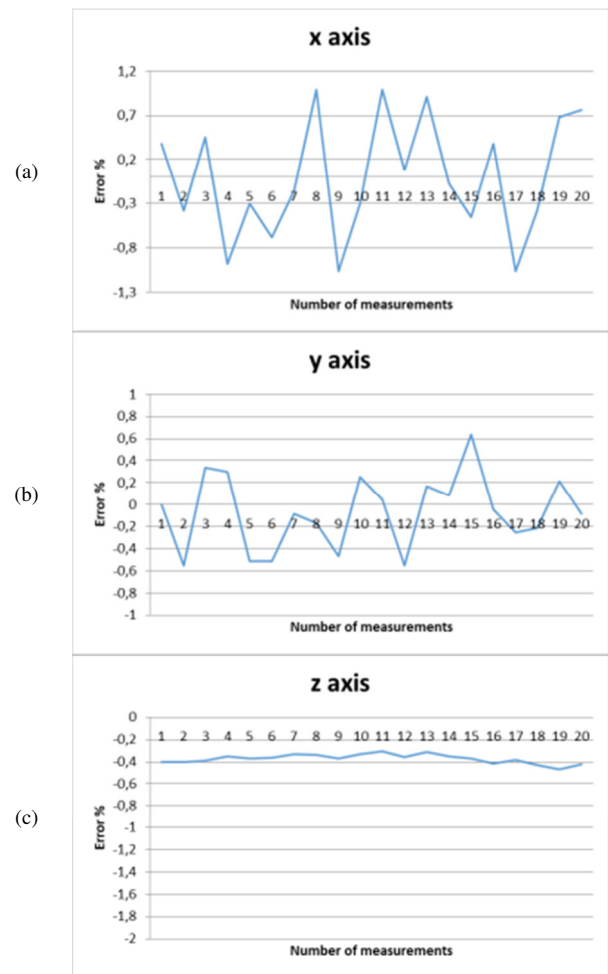


Fig. 15. Repeatability error.

In the literature, there are a few studies where commercial sensors are compared with the proposed sensors. These studies present small amounts of data and comparative assessment [43, 44].

Measurements were implemented on different axes after the commercial sensor was calibrated on the test platform. Experimental measurements were performed under the same conditions with the proposed sensor and the commercial sensor having been compared (Figure 16). For experimental comparison, the weight loading process described in the previous section was repeated with the commercial sensor. The measurement results in the vertical direction (z axis) are provided in Table VII.



Fig. 16. Measurements with a commercial sensor.

TABLE VII. COMPARISON OF SENSOR PACKAGE AND THE COMMERCIAL SENSOR FOR F_z

Input Force (N)	Output for proposed sensor		Output for Commercial sensor	
	Measured force (N)	Error ratio (%)	Measured force (N)	Error ratio (%)
47.02	46.67	0.75	47.09	0.14
93.91	93.26	0.69	95.26	1.44
143.06	142.92	0.10	143.73	0.47
190.43	189.59	0.44	189.17	0.66

Table VII manifests the error rates of the proposed and the commercial sensors. There is some error in the measurements of the commercial sensor. The suggested sensor displays higher accuracy for these measurements. It can be concluded that the former was verified from the comparison results. The comparative measurement results in Table VII are similar in terms of error ratios. The proposed sensor gives measurements with high accuracy, considering the error margin in both sensors.

VIII. CONCLUSION

Transfemoral prostheses must acquire accurate feedback about the ground reaction forces in order for the former to be controlled correctly. Transfemoral prosthetic sensors provide a precise way to estimate ground reaction forces for prosthetic users. Although there are many similar sensors, none of them is commercially employed, usually due its high costs. Just as almost every prosthesis is personalized, its sensor is also specifically manufactured to meet the needs of the prosthetic part. In the same way, the proposed sensor in this study is a new sensor specifically adapted to the designed transfemoral prosthesis.

In this study, a low-cost three-axis force sensor modularly designed is thoroughly presented. For the designed transfemoral prosthesis, the ground reaction forces below the ankle joint are accurately measured by the sensor. The proposed sensor is a much cheaper and more practical solution than other known sensors. The former consists of three main blocks: lower and upper mounting plates, upper and lower ABS plates, and four load cells. The lower and upper mounting plates and the upper and lower load cell spacers are made of laser-cut sheet metal and carbon fiber ABS material manufactured with 3D printers, respectively. The modular design of the sensor makes it simpler to be manufactured and assembled. By swapping out the load cells as needed, modular structural feature allows for easy adjustment of the detection limits. A control card, containing a microcontroller module, four load cell amplifiers, and an orientation sensor, is designed to receive sensor data. The simulation results obtained from the finite element analysis software (Table III) suggest that the sensor design provides sufficient strength.

In order to clearly indicate the contribution of this article, the proposed sensor was compared with an existing commercial sensor. According to the comparison results, the proposed sensor has advantages in some topics: (i) modular structure, (ii) less production and assembly complexity, (iii) lower cost, and (iv) integrated electronic and mechanical structures. The suggested sensor is a modular structured sensor, because the detection limits can be expanded according to the requirements

generated by changing the individual load cells. Given that it has a simple and modular structure, the complexity of production and assembly is less than the norm, rendering the proposed sensor cost-effective. Using low-cost methods in sensor production can significantly reduce the prosthesis sensor prices and support the widespread use of prostheses.

Some other characteristics of the proposed sensor are: (i) The orientation sensor already mounted on the electronic card will be used in a future study to detect angular forces in the prosthesis, (ii) the introduced sensor with its own microcontroller provides ease of control by reducing the processing load in prosthesis control experiments.

A test platform was constructed to measure the performance of the sensor package. Transfemoral prosthesis and ankle joint movements were also provided on the test platform. During the test, the forces were exerted to the sensor in the test platform at different angles of the ankle joint. The test results reveal that the sensor has precision sensitivity, low linearity error, and low interference error. These features are sufficient for using the proposed sensor in transfemoral prosthesis.

In addition, comparative measurements were performed with a commercial sensor for verification. The measurement results of the proposed sensor and the commercial sensor are highly coherent. The suggested sensor measures display high accuracy.

As a result of the tests performed, it is determined that the sensor is suitable for GRF measurement.

REFERENCES

- [1] J. Finch, "The complex aspects of experimental archaeology: the design of working models of two ancient Egyptian great toe prostheses," in *Prostheses in Antiquity*, London, UK: Routledge, 2018, pp. 29–48.
- [2] K. R. Kaufman, J. A. Levine, R. H. Brey, S. K. McCrady, D. J. Padgett, and M. J. Joyner, "Energy Expenditure and Activity of Transfemoral Amputees Using Mechanical and Microprocessor-Controlled Prosthetic Knees," *Archives of Physical Medicine and Rehabilitation*, vol. 89, no. 7, pp. 1380–1385, Jul. 2008, <https://doi.org/10.1016/j.apmr.2007.11.053>.
- [3] J. G. Penn-Barwell, "Outcomes in lower limb amputation following trauma: A systematic review and meta-analysis," *Injury*, vol. 42, no. 12, pp. 1474–1479, Dec. 2011, <https://doi.org/10.1016/j.injury.2011.07.005>.
- [4] J. M. P. de Godoy, D. M. Braile, S. H. G. Buzatto, O. Longo, and O. A. Fontes, "Quality of life after amputation," *Psychology, Health & Medicine*, vol. 7, no. 4, pp. 397–400, Nov. 2002, <https://doi.org/10.1080/1354850021000015212>.
- [5] R. Sinha and W. J. A. Van Den Heuvel, "A systematic literature review of quality of life in lower limb amputees," *Disability and Rehabilitation*, vol. 33, no. 11, pp. 883–899, Jan. 2011, <https://doi.org/10.3109/09638288.2010.514646>.
- [6] H. Senra, R. A. Oliveira, I. Leal, and C. Vieira, "Beyond the body image: a qualitative study on how adults experience lower limb amputation," *Clinical Rehabilitation*, vol. 26, no. 2, pp. 180–191, Feb. 2012, <https://doi.org/10.1177/0269215511410731>.
- [7] B. Rybarczyk, R. Edwards, and J. Behel, "Diversity in adjustment to a leg amputation: Case illustrations of common themes," *Disability and Rehabilitation*, vol. 26, no. 14–15, pp. 944–953, Jul. 2004, <https://doi.org/10.1080/09638280410001708986>.
- [8] A. Norlyk, B. Martinsen, and K. Kjaer-Petersen, "Living with clipped wings—Patients' experience of losing a leg," *International Journal of Qualitative Studies on Health and Well-being*, vol. 8, no. 1, Jan. 2013, Art. no. 21891, <https://doi.org/10.3402/qhw.v8i0.21891>.

- [9] W. Lovegreen, D. P. Murphy, P. M. Stevens, Y. I. Seo, and J. B. Webster, "Lower Limb Amputation and Gait," in *Braddom's Physical Medicine and Rehabilitation*, Sixth Edition., D. X. Cifu, Ed. Amsterdam, Netherlands: Elsevier, 2021, pp. 174-208.
- [10] L. Graham, M. Doherty, C. Wilson, C. Wilson, and M. Currie, "The multidisciplinary rehabilitation of patients after lower-limb amputation," *The Diabetic Foot Journal*, vol. 22, no. 3, 2019, Art. no. 32.
- [11] F. Sup, H. A. Varol, and M. Goldfarb, "Upslope Walking With a Powered Knee and Ankle Prosthesis: Initial Results With an Amputee Subject," *IEEE Transactions on Neural Systems and Rehabilitation Engineering*, vol. 19, no. 1, pp. 71-78, Feb. 2011, <https://doi.org/10.1109/TNSRE.2010.2087360>.
- [12] R. D. Bellman, M. A. Holgate, and T. G. Sugar, "SPARKy 3: Design of an active robotic ankle prosthesis with two actuated degrees of freedom using regenerative kinetics," in *2nd IEEE RAS & EMBS International Conference on Biomedical Robotics and Biomechatronics*, Scottsdale, AZ, USA, Oct. 2008, pp. 511-516, <https://doi.org/10.1109/BIOROB.2008.4762887>.
- [13] E. M. Ficanha and M. Rastgaar, "Preliminary design and evaluation of a multi-axis ankle-foot prosthesis," in *5th IEEE RAS/EMBS International Conference on Biomedical Robotics and Biomechatronics*, Sao Paulo, Brazil, Aug. 2014, pp. 1033-1038, <https://doi.org/10.1109/BIOROB.2014.6913916>.
- [14] M. Ege and S. Kucuk, "Energy Minimization of New Robotic-Type Above-Knee Prosthesis for Higher Battery Lifetime," *Applied Sciences*, vol. 13, no. 6, Jan. 2023, Art. no. 3868, <https://doi.org/10.3390/app13063868>.
- [15] M. Liu, F. Zhang, P. Datsersis, and H. (Helen) Huang, "Improving Finite State Impedance Control of Active-Transfemoral Prosthesis Using Dempster-Shafer Based State Transition Rules," *Journal of Intelligent & Robotic Systems*, vol. 76, no. 3, pp. 461-474, Dec. 2014, <https://doi.org/10.1007/s10846-013-9979-3>.
- [16] S.-K. Wu, G. Waycaster, and X. Shen, "Electromyography-based control of active above-knee prostheses," *Control Engineering Practice*, vol. 19, no. 8, pp. 875-882, Aug. 2011, <https://doi.org/10.1016/j.conengprac.2011.04.017>.
- [17] U. Mayetin and S. Kucuk, "Design and Experimental Evaluation of a Low Cost, Portable, 3-DOF Wrist Rehabilitation Robot with High Physical Human-Robot Interaction," *Journal of Intelligent & Robotic Systems*, vol. 106, no. 3, Nov. 2022, Art. no. 65, <https://doi.org/10.1007/s10846-022-01762-6>.
- [18] S. Kumar, M. Majeedullah, A. B. Buriro, and Rohibullah, "Autonomous Navigation and Real Time Mapping Using Ultrasonic Sensors in NAO Humanoid Robot," *Engineering, Technology & Applied Science Research*, vol. 12, no. 5, pp. 9102-9107, Oct. 2022, <https://doi.org/10.48084/etasr.5180>.
- [19] B. Kasmi and A. Hassam, "Comparative Study between Fuzzy Logic and Interval Type-2 Fuzzy Logic Controllers for the Trajectory Planning of a Mobile Robot," *Engineering, Technology & Applied Science Research*, vol. 11, no. 2, pp. 7011-7017, Apr. 2021, <https://doi.org/10.48084/etasr.4031>.
- [20] A. J. Young, T. A. Kuiken, and L. J. Hargrove, "Analysis of using EMG and mechanical sensors to enhance intent recognition in powered lower limb prostheses," *Journal of Neural Engineering*, vol. 11, no. 5, Jun. 2014, Art. no. 056021, <https://doi.org/10.1088/1741-2560/11/5/056021>.
- [21] A. Chadwell *et al.*, "Technology for monitoring everyday prosthesis use: a systematic review," *Journal of NeuroEngineering and Rehabilitation*, vol. 17, no. 1, Jul. 2020, Art. no. 93, <https://doi.org/10.1186/s12984-020-00711-4>.
- [22] F. H. Fahmi and S. Al-Zaidee, "Strength and Deflection Reliability Estimation of Girder Steel Portal Frames Using the Bayesian Updating Method," *Engineering, Technology & Applied Science Research*, vol. 12, no. 6, pp. 9584-9589, Dec. 2022, <https://doi.org/10.48084/etasr.5261>.
- [23] E. C. Martinez-Villalpando, H. Herr, and M. Farrell, "Estimation of Ground Reaction Force and Zero Moment Point on a Powered Ankle-Foot Prosthesis," in *29th Annual International Conference of the IEEE Engineering in Medicine and Biology Society*, Lyon, France, Aug. 2007, pp. 4687-4692, <https://doi.org/10.1109/IEMBS.2007.4353386>.
- [24] V. Azimi, T. T. Nguyen, M. Sharifi, S. A. Fakoorian, and D. Simon, "Robust Ground Reaction Force Estimation and Control of Lower-Limb Prostheses: Theory and Simulation," *IEEE Transactions on Systems, Man, and Cybernetics: Systems*, vol. 50, no. 8, pp. 3024-3035, Dec. 2020, <https://doi.org/10.1109/TSMC.2018.2836913>.
- [25] "ATI Industrial Automation: Multi-Axis Force / Torque Sensors." <https://www.ati-ia.com/products/ft/sensors.aspx>.
- [26] S. Pandit, A. K. Godiyal, A. K. Vimal, U. Singh, D. Joshi, and D. Kalyanasundaram, "An Affordable Insole-Sensor-Based Trans-Femoral Prosthesis for Normal Gait," *Sensors*, vol. 18, no. 3, Mar. 2018, Art. no. 706, <https://doi.org/10.3390/s18030706>.
- [27] R. Riemer, M. Rabuffetti, and C. Frigo, "Joint powers in stair climbing at different slopes," in *First Joint BMES/EMBS Conference. 1999 IEEE Engineering in Medicine and Biology 21st Annual Conference and the 1999 Annual Fall Meeting of the Biomedical Engineering Society*, Atlanta, GA, USA, Oct. 1999, vol. 1, Art. no. 530, <https://doi.org/10.1109/IEMBS.1999.802608>.
- [28] D. A. Winter, *Biomechanics and motor control of human gait: normal, elderly and pathological*, 2nd edition. Waterloo, ON, Canada: University of Waterloo Press, 1991.
- [29] J. Richards, A. Chohan, and R. Erande, "Biomechanics," in *Tidy's Physiotherapy*, S. Porter, Ed. Amsterdam, Netherlands: Elsevier, 2013, pp. 331-368.
- [30] P. Sardain and G. Bessonnet, "Gait analysis of a human walker wearing robot feet as shoes," in *ICRA. IEEE International Conference on Robotics and Automation (Cat. No.01CH37164)*, Seoul, Korea (South), May 2001, vol. 3, pp. 2285-2292 vol.3, <https://doi.org/10.1109/ROBOT.2001.932963>.
- [31] K. Nishiwaki, Y. Murakami, S. Kagami, Y. Kuniyoshi, M. Inaba, and H. Inoue, "A six-axis force sensor with parallel support mechanism to measure the ground reaction force of humanoid robot," in *IEEE International Conference on Robotics and Automation (Cat. No.02CH37292)*, Washington, DC, USA, Dec. 2002, vol. 3, pp. 2277-2282 vol.3, <https://doi.org/10.1109/ROBOT.2002.1013571>.
- [32] S. J. Morris, "A shoe-integrated sensor system for wireless gait analysis and real-time therapeutic feedback," Ph.D. dissertation, Massachusetts Institute of Technology, Cambridge, MA, USA, 2004.
- [33] C. Yuan, L.-P. Luo, K.-S. Shin, and C.-S. Han, "Design and analysis of a 6-DOF force/torque sensor for human gait analysis," in *13th International Conference on Control, Automation and Systems*, Gwangju, Korea (South), Oct. 2013, pp. 1788-1793, <https://doi.org/10.1109/ICCAS.2013.6704229>.
- [34] R. F. Lind, L. J. Love, J. C. Rowe, and F. G. Pin, "Multi-axis foot reaction force/torque sensor for biomedical applications," in *IEEE/RSJ International Conference on Intelligent Robots and Systems*, St. Louis, MO, USA, Oct. 2009, pp. 2575-2579, <https://doi.org/10.1109/IROS.2009.5353917>.
- [35] T. Liu, Y. Inoue, and K. Shibata, "A Wearable Ground Reaction Force Sensor System and Its Application to the Measurement of Extrinsic Gait Variability," *Sensors*, vol. 10, no. 11, pp. 10240-10255, Nov. 2010, <https://doi.org/10.3390/s101110240>.
- [36] "ATI Industrial Automation: F/T Sensor Nano25." https://www.ati-ia.com/products/ft/ft_models.aspx?id=Nano25.
- [37] P. H. Veltink, C. Liedtke, E. Droog, and H. van der Kooij, "Ambulatory measurement of ground reaction forces," *IEEE Transactions on Neural Systems and Rehabilitation Engineering*, vol. 13, no. 3, pp. 423-427, Sep. 2005, <https://doi.org/10.1109/TNSRE.2005.847359>.
- [38] S. J. Kim, G. M. Gu, Y. Na, J. Park, Y. Kim, and J. Kim, "Wireless Ground Reaction Force Sensing System Using a Mechanically Decoupled Two-Dimensional Force Sensor," *IEEE/ASME Transactions on Mechatronics*, vol. 25, no. 1, pp. 66-75, Feb. 2020, <https://doi.org/10.1109/TMECH.2019.2948650>.
- [39] L. Frossard, L. Cheze, and R. Dumas, "Dynamic input to determine hip joint moments, power and work on the prosthetic limb of transfemoral amputees: ground reaction vs knee reaction," *Prosthetics and Orthotics International*, vol. 35, no. 2, pp. 140-149, Jun. 2011, <https://doi.org/10.1177/0309364611409002>.

- [40] F. Sup, H. A. Varol, J. Mitchell, T. Withrow, and M. Goldfarb, "Design and control of an active electrical knee and ankle prosthesis," in *2nd IEEE RAS & EMBS International Conference on Biomedical Robotics and Biomechanics*, Scottsdale, AZ, USA, Oct. 2008, pp. 523–528, <https://doi.org/10.1109/BIOROB.2008.4762811>.
- [41] J. Park, S. J. Kim, Y. Na, Y. Kim, and J. Kim, "Development of a Bendable Outsole Biaxial Ground Reaction Force Measurement System," *Sensors*, vol. 19, no. 11, Jan. 2019, Art. no. 2641, <https://doi.org/10.3390/s19112641>.
- [42] U. Mayetin and S. Kucuk, "A low cost 3-DOF force sensing unit design for wrist rehabilitation robots," *Mechatronics*, vol. 78, Oct. 2021, Art. no. 102623, <https://doi.org/10.1016/j.mechatronics.2021.102623>.
- [43] J.-J. Park and G.-S. Kim, "Development of the 6-axis force/moment sensor for an intelligent robot's gripper," *Sensors and Actuators A: Physical*, vol. 118, no. 1, pp. 127–134, Jan. 2005, <https://doi.org/10.1016/j.sna.2004.07.013>.
- [44] Q. Liang, D. Zhang, Q. Song, Y. Ge, H. Cao, and Y. Ge, "Design and fabrication of a six-dimensional wrist force/torque sensor based on E-type membranes compared to cross beams," *Measurement*, vol. 43, no. 10, pp. 1702–1719, Dec. 2010, <https://doi.org/10.1016/j.measurement.2010.09.010>.
- [45] F. Paulsen and J. Waschke, *Sobotta Clinical Atlas of Human Anatomy*. Munich, Germany: Elsevier, 2019.
- [46] J. W. Guggenheim, L. P. Jentoft, Y. Tenzer, and R. D. Howe, "Robust and Inexpensive Six-Axis Force–Torque Sensors Using MEMS Barometers," *IEEE/ASME Transactions on Mechatronics*, vol. 22, no. 2, pp. 838–844, Apr. 2017, <https://doi.org/10.1109/TMECH.2017.2654446>.
- [47] G.-S. Kim, "Design of a six-axis wrist force/moment sensor using FEM and its fabrication for an intelligent robot," *Sensors and Actuators A: Physical*, vol. 133, no. 1, pp. 27–34, Jan. 2007, <https://doi.org/10.1016/j.sna.2006.03.038>.